Two-dimensional cochlear fluid model: New results

J. B. Allen

Acoustics Research Department, Bell Laboratories, Murray Hill, New Jersey 07974
(Received 29 March 1976; revised 20 September 20 1976)

Many theories have been developed in past years which have attempted to model the function of the human cochlea. With the recent availability of the physical measurements of Rhode [J. Acoust. Soc. Am. 49, 1218 (1971)], these theories now appear to be inadequate. In this paper, improved numerical solutions have been found for the two-dimensional cochlear model proposed by Lesser and Berkley [J. Fluid Mech. 51, 497 (1972)], using the Green's-function method as first suggested by Cox and Lien [(1973) unpublished]. The Green's-function method is used to derive an integral equation which may then be solved numerically. This procedure has proven to be stable, accurate, and faster than several other numerical solution techniques that have been tried. With an appropriate selection of the assumed membrane dissipation, the results are seen to agree within a few decibels of the Mössbauer measurements of Rhode, including the sharp change in slope observed in his amplitude ratio measurements just above the best frequency. This plateau occurs at a level which is 58 dB lower in amplitude than the amplitude at the best frequency.

PACS numbers: 43.63.Bq, 43.63.Kz

LIST OF SYMBOLS

ϕ	velocity potential,
$\mathbf{V}$	velocity vector (V_x, V_y),
p	pressure,
f	natural frequency,
ω	radian frequency,
ρ	density,
i	$\sqrt{-1}$,
$K(x)$	stiffness parameter,
$R(x)$	loss parameter,
M	mass parameter,
Z	impedance,
V_{BM}	$-V_y$ component of V_n,
V_n	normal velocity,
$\mathbf{X}$	(x,y) vector
λ	wavelength,
G	Green's function,
G_{BM}	Green's function evaluated on basilar membrane,
L, H, W	dimensions of cochlear chamber,
a	exponential constant in $R(x)$.

INTRODUCTION

Much attention has been focused in the literature over the past several years on the problem of the mechanical response of the basilar membrane to an acoustic signal stimulation. von Békésy (1960) was the first to measure physical motion of basilar membrane. Recently, Rhode (1971), Johnstone and Boyle (1967), and Rhode and Robles (1974), have given us more detailed and accurate data using a radioactive Mössbauer source while Wilson and Johnstone (1972) have developed a capacitive probe technique. These physical data show detailed effects which have not been observed either in von Békésy's data or in any theoretical calculations.

Various attempts toward understanding von Békésy's data have led to the development of one-dimensional transmission-line theories (Zwislocki, 1965; Peterson and Bogert, 1950; Schoeder, 1973; and Zweig *et al.*, 1976) based on von Békésy's observations of a traveling wave on the membrane.

More sophisticated and complete theories have been advanced in the literature, again based on von Békésy's original results, but these models have not been probed in depth. The more complete theories include two- and three-dimensional fluid dynamical or quasistatic models. Steele (1974) has proposed several models but has not yet compared the results directly to the physical data. Lien and Cox (1973) developed a detailed three-dimensional model but then reduced it to the previously derived and well-known one-dimensional transmission-line model after several simplifying assumptions. Siebert (1974), in the spirit of Ranke (1950), developed a two-dimensional model which he then simplified by making a short-wavelength approximation. His solutions are believed to be useful only near the place of best frequency. Lesser and Berkley (1972) formulated a two-dimensional fluid model which they solved numerically. Their solution would appear to be the most complete among these multidimensional models since these were obtained directly from the model by numerical methods. However their numerical results were limited and were highly sensitive to computational errors.

The one-dimensional models proposed to date (Zwislocki, 1965: Peterson and Bogert, 1950; Schroeder, 1973; Zweig *et al.*, 1976) have not been correctly based on direct physical measurements of basic constants, such as the elasticity of tissue, because of the problem of relating these fundamental constants to the model's transmission-line impedance. The multidimensional models have been only slightly more successful in this regard due to the great difficulties in obtaining these data and due to the lack of knowledge of the important mechanisms. For example, detailed knowledge of the restoring forces within the basilar membrane, or of any system loss mechanisms, have been matters of conjecture. Lien and Cox (1973), Allarie *et al.* (1974), Steele (1974),

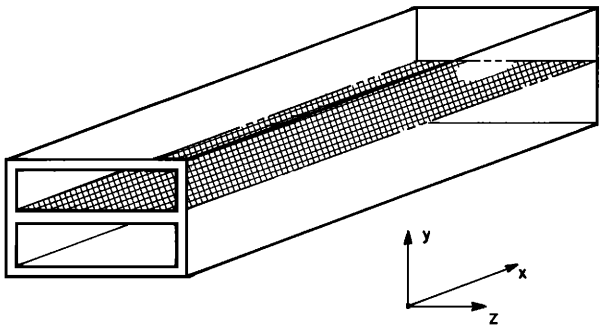

FIG. 1. Mathematically idealized model of the cochlea. The oval and round windows are be on the left end while the helocitrema may be seen on the right end. The basilar membrane is represented by the cross-hatched region.

and Novoselova (1975) concerned themselves with these problems of basic mechanisms, and in the cases of Allarie and Novoselova, have ignored temporarily the fluid aspects of the problem in order to gain a deeper understanding of the basic principles.

Ultimately, nonlinear effects are of interest (Kim *et al.*, 1973; Hall, 1974; Schroeder, 1975). If we are to gain any understanding in the future of these nonlinear effects thought to be present in basilar-membrane motion, a thorough understanding of the underlying phenomenon is essential.

I. PRESENT APPROACH

Because of the many approaches and approximations described above, considerable confusion exists in the field as to which features of the various models are essential. A controversy has long existed with regard to the relative merits of single versus multidimensional theories (long- versus short-wavelength problem).

This paper presents an accurate numerical solution of a particular two-dimensional model. First the results are given and then the method of analysis is carefully developed, since it is the only numerically acceptable procedure known to the author for solving the full equations with accuracy and stability. We will demonstrate that the present theory is in closer agreement with the physical measurements of Rhode (1971) than the one-dimensional theory. Results from one-dimensional models qualitatively deviate from results of two-dimensional models due to differences in the response at the best frequency and the plateau in the magnitude response above the place. These deficiencies are believed to be inherent in transmission-line models. No reasonable one-dimensional theory is believed to exist which is totally acceptable. This is not to say that one-dimensional models are not useful in many approximate applications.

II. SUMMARY OF EQUATIONS AND RESULTS

We shall now summarize the equations of the model and compare the solutions to both Rhode's data (1971) (animal 69-473) and to one-dimensional solutions. Because of the variability in the experimental data, and the computation time involved, more comparisons have not been attempted.

An uncoiled cochlea is physically similar to the box shown in Fig. 1 where rectangular coordinates have been assumed for simplicity (Lesser and Berkley, 1972). The basilar membrane splits the fluid-filled box down the center as is indicated in the drawing by the shaded region. The stapes is connected to the upper rectangular region shown in the left and acts like a piston driving the fluid in and out. The lower window is assumed at all times to be exactly out of phase such that when the upper piston is moving in, the lower piston is moving out.

The fluid is assumed to be incompressible (no change in fluid density). This assumption implies an infinite speed of sound in the fluid, an approximation which is valid because the distance from the stapes to the point of maximum displacement is much less than the wavelength of sound in the fluid (Lesser and Berkley, 1972). We also assume that the fluid is inviscid. The loss will be introduced as internal friction within the basilar membrane.

Thus for a steady-state complex sinusoidal excitation at the stapes of radian frequency ω, the fluid motion may be described by the following equations:

$$\nabla^2\phi = 0 \ , \tag{1}$$

$$V = -\nabla\phi \ , \tag{2}$$

and

$$p = i\omega\rho\phi \ . \tag{3}$$

The cochlea may be unfolded (Lesser and Berkley, 1972; Lien and Cox, 1973) as shown in Fig. 2(b). The stapes boundary condition is defined as a spatially uniform, single frequency velocity source (assumed here to be 1 cm/sec). At the helicotrema, the potential is assumed to be zero. On the upper wall at $y = H$, $V_y = 0$

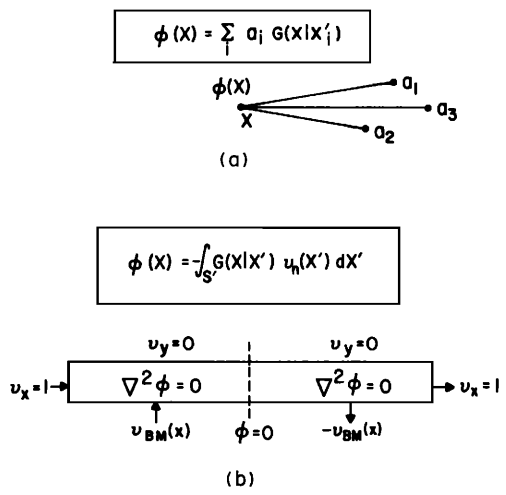

FIG. 2. (a) When a distribution of point sources is known, the potential may be determined by superposition. (b) Unfolded mathematical idealization showing velocity boundary conditions. The equations relate the velocities to the potential by the use of superposition of the Green's function $G(X|X')$.

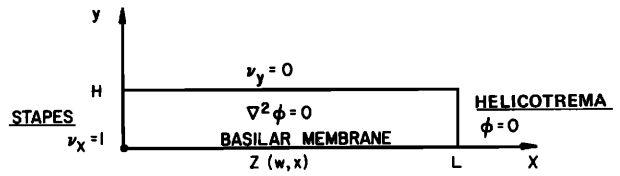

FIG. 3. Physical model and boundary conditions.

since no fluid may flow through this boundary.

The boundary condition on the basilar membrane (BM), namely at $y = 0$, is derived in Appendix C. It relates the pressure p to the BM velocity V_{BM}:

$$p/V_{BM}|_{y=0} = K(x)/i\omega + R(x) + i\omega M \ , \qquad (4)$$

where $K(x)$ is the BM's stiffness due to its transverse bending moment, $R(x)$ is the loss, and M is the BM's mass. $R(x)$, the loss term, is the only parameter which has not been independently measured. It is therefore chosen to be in agreement with the measured data of Rhode (1971).

The solution of our problem is thus given in terms of the velocity potential $\phi(x, \omega)$ on the BM as a function of frequency. The velocity V_{BM} may be found from Eqs. (3) and (4).

V_{BM} has been plotted for various frequencies in Fig. 8. It is interesting that ϕ is a complex variable and that because of (1), defines an analytic function of the complex variable $x + iy$ inside the fluid-filled chamber.

An immediately useful result is the approximate proportionality between log frequency and characteristic place.[1] Note in Fig. 8 that one octave in frequency always corresponds to the same distance. For example, the distance between the places at 100 and 200 Hz is the same as the distance between the places for 5 and 10 kHz. Using this relationship, we may transform the velocity as a function of x for one frequency into the velocity as a function of frequency at one place. Since Rhode's (1971) data have already been plotted on a log-frequency scale, his data need only be scaled linearly along the ordinate and the abscissa in order to be compared to our computed results.

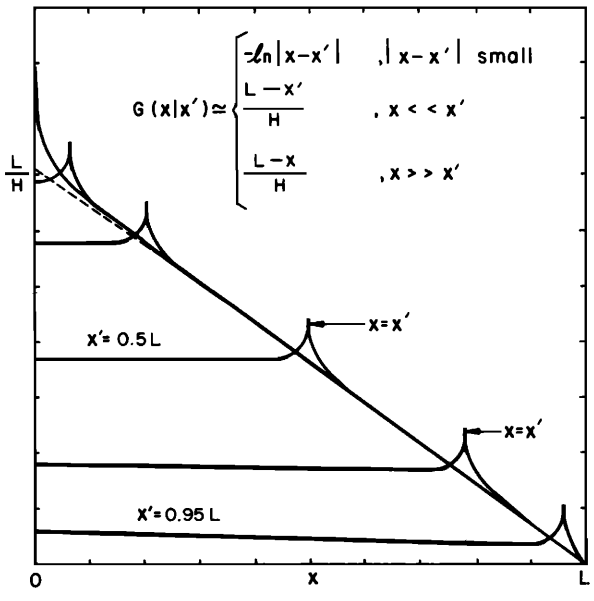

FIG. 4. Plot of the Green's function $G_{BM}(x|x')$ for various values of x'.

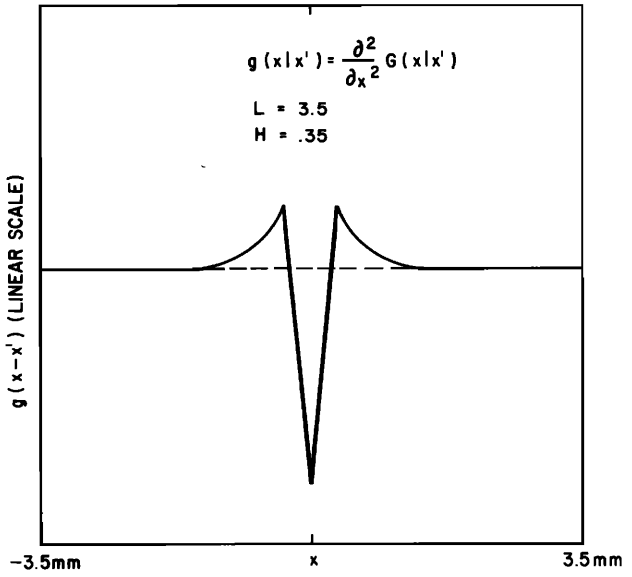

FIG. 5. Plot of the second difference of $G_{BM}(x|x')$ as a function of $x-x'$. The second difference simulates the second derivative.

The approximate frequency shift-invariant property that we have observed above can also be observed in the one-dimensional model. From that model we may determine the transformation between the frequency data and the place data. This transformation, which has been numerically verified using a one-dimensional model is

$$f = f_0 e^{ax} \ . \qquad (5)$$

The constant a must be identically equal to the exponential factor of the resistance term in the BM impedance $R(x)$. In our simulations, a was chosen to be 1.7.

Shift invariance of the velocity envelope implies a linear cochlear map. The cochlear map is a plot of the characteristic place as a function of the logarithm of the frequency. When the cochlear map is not linear, the transformation between the frequency response and the place response is more complex. Since we have assumed a linear cochlear map in our model and have chosen parameters which are consistent with shift invariance, the model results remain the same on either the x or $\log(f)$ scale. Experimental observations only satisfy these assumptions over a limited range however, thus slow variations between our results and Rhode's (1971) data are expected.

We therefore transformed Rhode's data from frequency to place using the exponential transformation with a equal to the value chosen in the impedance calculation.

It should be stressed that this approximation is exact when the cochlear map is linear and shift invariance holds. This result is plotted in Fig. 6. In that figure we see a comparison between our result, Rhode's (1971) data, and Zweig *et al.*'s (1976) one-dimensional-model results.

The agreement between Rhode's and our results close both quantitatively and qualitatively. Note the sharp discontinuity in the magnitude function above the characteristic place. This detail, which is 58 dB down relative to the peak, has not been reproduced in any one-dimensional model.

The phase data are not easily compared without massive calculations. Each frequency point requires a two-hour calculation to do the matrix inversion for a 200-point solution. Thus using the present solution technique, a limited amount of results are necessary. Rather than proceeding with the present solution technique, we are investigating more efficient models which maintain adequate accuracy compared to the original model.

Rhode's (1971) phase and magnitude as a function of $\log(f)$ is shown in Fig. 7(a). The phase and magnitude for our results as a function of x is shown in Fig. 7(a). Only the end points may be compared directly. Our phase has a total accumulation of 6π while Rhode's phase accumulation is 9π. The phase accumulation appears to be highly correlated with the plateau to peak ratio in the magnitude response. Thus we could not match both aspects of the curves simultaneously. The conditions for this experiment are given in (C12) (see Appendix C). More accurate numerical results are necessary to determine the true extent of this problem.

The plateau-to-peak ratio is almost entirely determined by the channel depth H and the membrane mass M. It is also slightly dependent on R, the loss. The

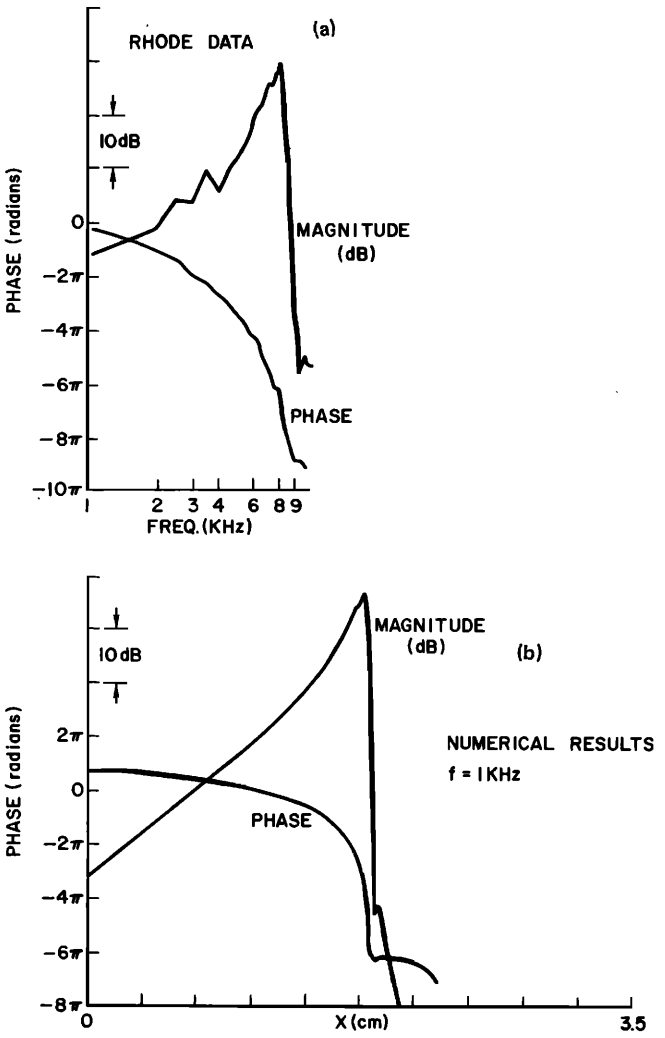

FIG. 7. The model phase and magnitude results and Rhode's measured phase and magnitude plotted as a function of $\log(f)$.

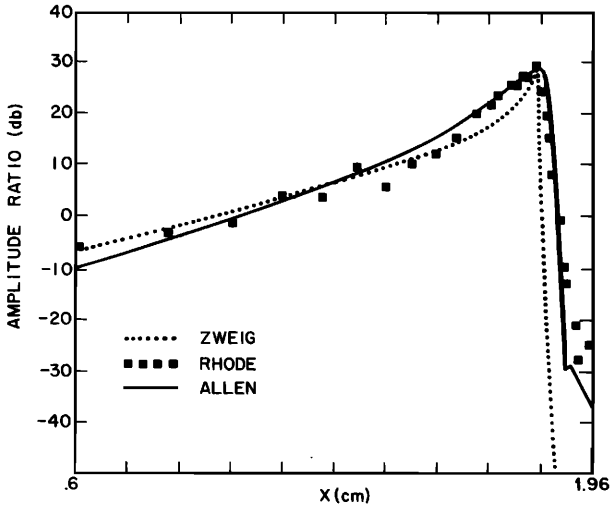

FIG. 6. Plots of the displacement ratios on the basilar membrane as a function of x or Log(f). The dots are the measured results of Rhode animal 69-473. [The Rhode data were taken from Fig. 4 of (Zweig *et al.*, 1976). The dotted curve is the one-dimensional result of Zweig, Lipes, and Pierce (1976).] The solid curve is the result of solving Eq. (13).

shape of the region around the place is determined almost entirely by M and R. Smaller R caused a sharp peak to rise at the place. Increasing M causes peaking and broadens the peak. Thus by carefully choosing H, M, and $R(x)$, the Rhode (1971) data may be matched as shown in Fig. 6. K and a, the stiffness and the exponential constant in R, are solely determined by the cochlear map.

We did not anticipate the critical interaction between the membrane mass M and the channel depth H. The velocity response is highly sensitive to the choice of these two parameters. A factor of two is qualitatively a large change.

We now proceed by developing a more complete derivation of the equations just discussed and our method of their solution is outlined.

III. PROBLEM FORMULATION-DIFFERENTIAL EQUATIONS

The model and approach we have chosen closely parallels and builds on two previous approaches, namely those of Lien and Cox (1973) and of Lesser and Berk-

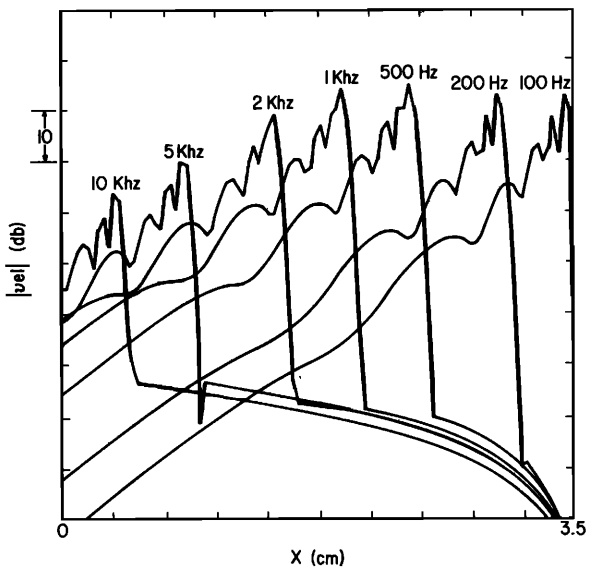

FIG. 8. Family of theoretical response curves for various frequencies as a function of position along the basilar membrane. These solutions were computed using 100 points. For this calculation, $L=3.5$, $H=0.35$, $K_0=10^9$, $R_0=100$ and $a=1.5$. If more points had been used, the ripples would not be present. Note that for steady state conditions, velocity ratios are equal to displacement ratios.

ley (1972). Lien and Cox have derived a model from basic principles which is essentially the model assumed at the onset by Lesser and Berkley. The latter go on to find numerical solutions, while the former reduced their equations to a one-dimensional transmission-line theory.

As previously described, the unrolled cochlea is similar to the idealization shown in Fig. 1. The sound velocity for the fluid filling the chambers is not known precisely, but is not much different from that of water. If we define the distance from the stapes to the place as D, and the wavelength in water for a frequency f as λ, then for all frequencies of interest

$$D/\lambda \ll 1. \tag{6}$$

Because the characteristic length D is much less than a wavelength, pressure changes applied at the oval window are immediately transferred to all parts of the system with a velocity which is infinite. This means that the wave equation is unnecessary in describing fluid motion and Laplace's equation will suffice.[2]

Next the cochlea is unfolded, by separating it along the basilar membrane with the hinge point at the apex $x=L$, and stretched so that the two chambers make one long chamber, as shown in Fig. 2(b). This model is equivalent to the folded one as long as we constrain the membrane velocity to be antisymmetric about the $x=L$ point (Lesser and Berkley, 1972; Lien and Cox, 1973). The steady-state fluid equations therefore reduce to Eqs. (1)–(3).

Equation (1) is just the result of conservation of mass

$$\nabla\cdot(\rho V)=0\ . \tag{7}$$

Equation (2) is the definition of the velocity potential. This equation is applicable because the curl of the velocity is assumed to be zero (no vorticity). Equation (3) is the result of Newton's law.

Associated boundary conditions are (1) the normal velocity on the upper wall is zero, (2) on the stapes end the fluid is driven with unit sinusoidal velocity, and (3) at the antisymmetric point $x=L$ the potential is zero.[3]

Finally, we must find a relation between the pressure and velocity on the basilar membrane in order to properly apply boundary conditions on this surface. The boundary conditions, except on the BM ($y=0$ plane) are therefore

$$\partial\phi/\partial x\big|_{x=0}=-1\ , \tag{8}$$

$$\phi\big|_{x=L}=0\ , \tag{9}$$

$$\partial\phi/\partial y\big|_{y=H}=0\ . \tag{10}$$

Equation (8) is the oval-window driving condition, (9) the antisymmetry condition, and (10) is the top rigid-wall condition.

Beside Eqs. (1)–(3) and (8)–(10) we also need the $y=0$ boundary condition on the BM [Eq. (4)] which is derived in Appendix C. This final boundary condition is the heart of the model, since it is the restoring force of the BM working against the mass of the fluid which causes the resonant behavior we wish to describe. Thus on the BM we assume the homogeneous mixed boundary condition given by Eq. (4).

IV. DERIVATION OF AN INTEGRAL EQUATION FORMULATION

We now transform our problem into an equivalent integral equation by the Green's function method. We do this formally in Appendix D, but in this section we present the needed results in a more intuitive manner.

Assume we have several point sources of magnitude a_n placed at locations X_n' as shown in Fig. 2(a). If the potential at X for a unit source at X_n' is $G(X|X_n')$ then the total potential is the weighted sum over all the sources, as shown in Fig. 2(a). The upper case X is used here to denote the coordinate pair (x,y) while the lower case x is the x-coordinate value.

Assuming velocity sources, the velocity potential[4] may be found by summing over all sources, thus defining an integral relationship between the potential, at any interior point X, and the normal velocity, on the boundary S' [Fig. 2(b)]

$$\phi(X)=-\int_{S'} G(X|X')V_n(X')dS'\ , \tag{11}$$

where $G(X|X')$ is a known function which must satisfy the boundary conditions of zero normal velocity on S'.

If we let $y=0$ in Eq. (11) we get an integral relationship between the potential and the velocity of the fluid V_{BM} *on the basilar membrane.* For $y=0$, we define $G_{BM}(x|x')=G(x,0|x',0)$. The evaluation of $G_{BM}(x|x')$ is given in Appendix B. Appendix A is a Fortran program

which may be used to evaluate $G_{BM}(x|x')$ numerically. In this program GR is an array containing the Green's function as a function of x assuming a source at point $IX0$. NX and NY are the limits of the image summation, NP is the number of x points used along the length, and XL and YL are the dimensions of the cavity in centimeters. For our simulations $XL = 3.5$, and $YL = 0.1$. M. M. Sondhi of Bell Telephone Laboratories has been able to sum our series and has found a closed-form solution for $G_{BM}(x|x')$. We evaluated his analytical result rather than numerically determining G_{BM}. The integral of G over the round- and oval-window ends may be evaluated exactly (Appendix B) and turns out to be the trivial result $L - x$. Thus Eq. (11) finally reduces to

$$\phi(x) - 2\int_{x'=0}^{L} G_{BM}(x|x')V_{BM}(x')dx' = L - x \ . \tag{12}$$

This integral relation relates the potential $\phi(x)$ to the velocity $V_{BM}(x)$ on the basilar membrane. All fluid properties and boundary conditions of the model have been included in this equation, and the only unused piece of information is the BM boundary condition given by Eq. (4).

Incorporating (4) into (12) reduces our problem to the solution of the integral equation

$$\phi(x) + 2i\omega\rho\int_{x'=0}^{L} G_{BM}(x|x')\frac{\phi(x')}{Z(x',\omega)}dx' = L - x \ . \tag{13}$$

V. NUMERICAL SOLUTIONS

In order to find solutions to Eq. (13) we used the finite-difference method (trapezoidal rule) to generate a discrete set of linear equations. Gaussian elimination was then used to solve the resulting matrix equation on a Data General S/200 Eclipse digital computer.

From experience, we found that a minimum of 100 points is needed to represent the data, thus the minimum size of the matrix equation must be at least 100×100. If 200 points were used, the solution did not differ by more than 3 dB from the 100-point solutions. In order to solve a set of equations this large, the equations were stored on disk and only two rows of the matrix were in core at one time. The Green's function was computed in advance and stored on disk. Note that since the Green's function is not a function of frequency, it need only be computed once.

Each frequency computation required a new evaluation of the matrix elements and a matrix inversion. The solution values were then put on disk or magnetic tape. The total time required at each frequency for a solution of 100 points was approximately twenty minutes on the Eclipse S/200 using moving head disks. It was crudely estimated that the computation time went as n to the fourth power, where n is the number of points in the matrix equation. Since there seemed to be no problem with accuracy, only single precision floating point was necessary, which on the Eclipse consists of a 32-bit floating-point word (24-bit mantissa with an 8-bit exponent).

Some tricks were used which were felt to be useful. First, since the Green's function is singular at $x = x'$, the finite difference at that point must be integrated analytically. Thus the effective diagonal value of the Green's function is found as follows:

$$G_{eff}\big|_{x=x',\Delta} = \int_{-\Delta/2}^{\Delta/2} \ln|x|\,dx \tag{14}$$

or

$$G_{eff}\big|_{x=x'} = \ln(\Delta/2) - 1 \ . \tag{15}$$

This correction has been included in the FORTRAN program of Appendix A.

The second trick was to take a second difference before solving the equations. This was done for several reasons. First, it allowed the boundary conditions to be reintroduced into the equations, thereby hopefully improving the global properties of the solutions (i.e., reduce the amount of error propagation in the recursive solution). The differenced set of equations were no harder to solve and seemed to be slightly better behaved in the region about $x = L$. (Note that since the Green's function would become non-integrable if its second derivative were taken, one must proceed carefully, as has been done by differencing the discrete set of equations.)

We have defined a function g as the second difference of G_{BM}. This new function is plotted in Fig. 5 over the restricted range of $\pm 10\%$ of the full length about the diagonal $x = x'$. It is interesting that $g(x|x')$ is approximately symmetrical; also it is a function only of the variable $x - x'$ to a good approximation except near the boundary points $x' = 0$ and $x' = L$. If the function $g(z)$ were a delta function at $z = 0$, then Eq. (13) could be exactly reduced to a transmission-line theory. If $g(z)$ is expanded as the second derivative of a delta function plus a delta function, it may still be reduced to a transmission-line theory. This was the approach of Lien and Cox (1973). All deviations from transmission-line behavior are due the nonlocal nature of $g(z)$. In comparing the present solutions to those of Zweig *et al.* (1976) as shown in Fig. 6, we see that near the place the differences are significant. Zweig did not use the same impedance values we used. He chose them to agree with the Rhode (1971) data. When our impedance values are used in the one-dimensional model, the resulting differences are even greater than those of Zweig.

VI. SUMMARY

We have presented a two-dimensional model in detail and shown that the solutions agree very closely to the physical measurements of Rhode. The two-dimensional model was reduced to an integral equation (13) which was solved numerically. We have noted that the difference between our model and the one-dimensional models has arisen because of the logarithmic behavior of the Green's function near $x = x'$.

Since all of the system parameters appear with greater physical meaning than those of a one-dimensional model, it might be possible to physically determine the source of the combination tone nonlinearity (Kim *et al.*, 1973; Hall, 1974; Schroeder, 1975). From the numerical work of others (Kim *et al.*, 1973; Hall, 1974; Hubbard and Geisler, 1972), it would appear that the non-

linearity may somehow be related to the loss term $R(x)$ in the basilar-membrane boundary condition. If the nonlinearity measured by Rhode and Robles (1974) is the same as the nonlinearity which causes the combination tones, then the Rhode (1971) data lends support to this hypothesis because increased loss would imply increased bandwidth. It is also clear that a more direct measurement of the loss term would be useful since the mechanism presented in Appendix C has been hypothetically chosen, due to a lack of any direct experimental evidence.

Little effort has been spent in this paper evaluating the qualitative effects seen to be present in the data, such as the plateau in the magnitude function above the characteristic place. An analytical interpretation of this phenomenon would be interesting. It is a two-dimensional effect which will not be present in one-dimensional models.

ACKNOWLEDGMENTS

Many people have been helpful throughout the conduct of this work. In particular I would especially like to thank D. A. Berkley for introducing me to this problem and for his help and insight. I also am indebted to J. S. Courtney Pratt for his encouragement and understanding, to M. M. Sondhi, and to J. R. Cox and W. M. Siebert for extensive comments.

APPENDIX A

```
C  PROGRAM NAME:  G4
C  COMPUTES GREEN'S FUNCTION FOR POINT IX0
C
      SUBROUTINE G4 (GR, IX0, NX, NY, NP, XL,YL)
      DIMENSION GR(1)
      TPY = 8.*ATAN(1.)
      DX = XL/FLOAT(NP-1)
      EXM1 = EXP(-1.)
      AS = (EXM1*DX/2.)**2
      TYL = 2.*YL
      FXL = 4.*XL
      TXL = 2.*XL
      NI = 2*NX+1
      NJ = 2*NY+2
      X00 = DX*FLOAT(IX0-1)
C  LOOP OVER X
      DO 20 IX = 1, NP
      GI = 0
      X = DX*FLOAT(IX-1)
C  LOOP OVER Y0
      DO 15 J = 1,NJ
      M = J-NY-1
      Y0 = TYL*FLOAT(M)
      Y02 = Y0**2
      G4 = 1
C  LOOP OVER X0
      DO 10 I = 1,NI
      N = I-NX-1
      X0 = X00+FXL*FLOAT(N)
      A1 = (X-X0)**2+Y02
      IF(A1.EQ.0.)A1 = AS
      A2 = (X+X0)**2+Y02
      IF(A2.EQ.0.)A2 = AS
      B1 = (TXL-X-X0)**2+Y02
      IF(B1.EQ.0.)B1 = AS
      B2 = (TXL-X+X0)**2+Y02
      IF(B2.EQ.0.)B2 = AS
      R4 = (A1*A2)/(B1*B2)
      G4 = G4*R4
   10 CONTINUE
      GI = GI-ALOG(G4)
   15 CONTINUE
      GR(IX) = GI/TPY
   20 CONTINUE
      RETURN
      END
```

APPENDIX B: BEHAVIOR OF THE GREEN'S FUNCTION

The Green's function used in Eq. (13) is the solution of the differential equation

$$\left(\frac{\partial^2}{\partial x^2}+\frac{\partial^2}{\partial y^2}\right)G(X|X')=-\delta(X-X') \tag{B1}$$

since we assume a two-dimensional model. Physically G is the potential at X due to a unit velocity source at X'. The upper case X used here represents the vector coordinates (x,y).

The two-dimensional Green's function in an unbounded region is given by

$$G(X|X')=-(2\pi)^{-1}\ln(|X-X'|). \tag{B2}$$

When the source is on a single rigid wall (zero normal velocity), the Green's function may be found by the method of images to be

$$G_{\text{wall}}(X|X')=-\pi^{-1}\ln(|X-X'|). \tag{B3}$$

Finally when the upper rigid wall and side walls are included, we may again use the method of images. However in this case, an infinite number are required as shown in Fig. 9, where a small portion of the infinite image space is presented (Morse and Feshbach, 1953). The source is introduced at $x=x'$, $y=0$. There is a positive image at $-x'$. Each of these two sources is periodically repeated with a period of $4L$ along the x axis. Negative images occur at $2L\pm x'$, also with a period of $4L$. Images also occur at multiples of $2H$.

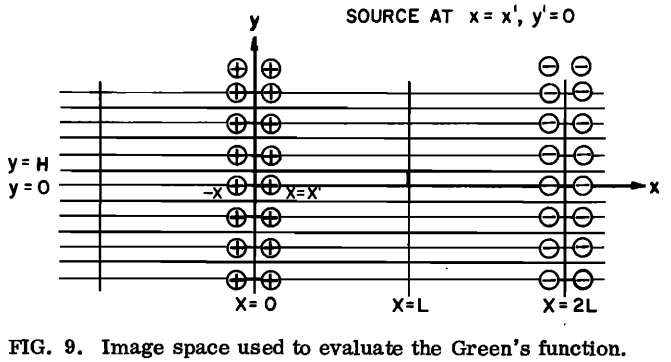

FIG. 9. Image space used to evaluate the Green's function. $G_{BM}(x|x')$ is found by summing over all images with the observation point restricted to the $y=0$ surface (line). The images are periodic with a period of $4L$ along x.

Since each image has a strength, other than sign, given by (B3), the full Green's function at $y=0$ is then

$$G_{BM}(x|x') = \frac{-1}{\pi} \sum_{n=-\infty}^{\infty} \sum_{m=-\infty}^{\infty} (-1)^n \ln(r_{nm}^{+} r_{nm}^{-}) , \quad \text{(B4)}$$

where

$$r_{nm}^{\pm} = [(x \pm x' + 2nL)^2 + (2mH)^2]^{1/2} \quad \text{(B5)}$$

Note that

$$r = |x| = (x^2+y^2)^{1/2} .$$

In practice this sum may be truncated after a few terms. In the solutions presented in Fig. 8, n and m were summed over ± 10 terms. $G_{BM}(x|x')$ for several values of x' are shown in Fig. 4.

To evaluate the integral when the source is at the oval window, images appear with a period of $2L$ and $2H$. For this case we find that at $y=0$

$$G_s(x|y') = \frac{-1}{\pi} \sum_{n=-\infty}^{\infty} \sum_{m=-\infty}^{\infty} (-1)^n \ln(r_{nm}^{+} r_{nm}^{-}) , \quad \text{(B6)}$$

where

$$r_{nm}^{\pm} = [(y' \pm 2mH)^2 + (x+2nL)^2]^{1/2} . \quad \text{(B7)}$$

Since the stapes source velocity is uniform, the integration over uniformly distributed line sources gives a uniform plane source. Thus we may evaluate the driving function integral exactly

$$2\int_{y'=0}^{H} G_s(x|y')\,dy' = L - x . \quad \text{(B8)}$$

Equation (B8) is the solution of the problem of finding the electrical potential between two uniformly charged plates. In our case, the charges are replaced by uniform, plane velocity sources and sinks.

APPENDIX C: DERIVATION OF IMPEDANCE BOUNDARY CONDITION

In this section we wish to derive the boundary conditions needed at the basilar-membrane surface $y=0$. This derivation was inspired by the one given by Lien and Cox (1973). It is believed by the author that more work needs to be done in this area. This section should be thought of as indicative of how this calculation might proceed.

We assume that the BM is an nonisotropic inhomogeneous plate vibrating with a known displacement distribution in the z dimension (a third dimension for this model). The differential equation relating h, the y displacement, to the forces on the plate is

$$D_z \partial^4 h(x,z)/\partial z^4 = f_n , \quad \text{(C1)}$$

where D_z is the stiffness parameter, h the y displacement, and f_n is the force normal to the plate (Timoshenko and Woinowsky-Krieger, 1959). Casual numerical experiments showed that the main effect of longitudinal stiffness was to dramatically reduce the sharp slope above the best frequency. Thus longitudinal stiffness was dropped from the model. The forces acting on the plate are due to the pressure of the fluid, the inertial mass of the plate, and internal friction of the plate.

The internal frictional forces are assumed to be proportional to the rate of curvature. Thus (C1) becomes

$$D_z(\partial^4 h/\partial z^4) = -2P + \omega^2 m h + i\omega r(\partial^2 h/\partial z^2) \quad \text{(C2)}$$

where P is the pressure, m is the membrane mass per unit area, and r is the internal loss coefficient.

Next we assume that the distribution of the displacement, and thus the velocity, is first-mode-like

$$h(x,z) = (V_{BM}(x)/i\omega)\cos[\pi z/W(x)] , \quad \text{(C3)}$$

where $W(x)$ is the width of the BM.

From (C2) and (C3) one may easily show that

$$\frac{P(x,z)}{V_{BM}(x)} = -\left[\frac{D_z \pi^4}{2i\omega W^4(x)} + \frac{i\omega m}{2} + \frac{r\pi^2}{2W^2(x)}\right]\cos\left(\frac{\pi z}{W(x)}\right) . \quad \text{(C4)}$$

If we integrate (C4) from $-W/2$ to $W/2$ after multiplying by $\cos[\pi z/W(x)]$ and then make the following definitions:

$$p(x) = \frac{2}{\pi}\int_{-W/2}^{W/2} P(x,z)\cos\left(\frac{\pi z}{W(x)}\right) dz , \quad \text{(C5)}$$

$$K(x) = D_z \pi^4/2W^4(x) , \quad \text{(C6)}$$

$$M = m/2 , \quad \text{(C7)}$$

$$R(x) = r\pi^2/2W^2(x) , \quad \text{(C8)}$$

$$Z(x,\omega) = -p(x)/V_{BM}(x) , \quad \text{(C9)}$$

we find the following expression for $Z(x,\omega)$, the effective BM impedance function

$$Z(x,\omega) = \frac{K(x)}{i\omega} + i\omega M + R(x) \quad \text{dyn sec/cm}^2 . \quad \text{(C10)}$$

For the solutions given here the following constants may be found

$$\begin{aligned} &W(x) = 0.017e^{0.85x} \text{ cm} , \\ &L = 3.5 \text{ cm} , \\ &H = 0.1 \text{ cm} , \\ &D_z = 1.7149 \text{ dyn cm} , \\ &m = 0.1 \text{ g/cm}^2 , \\ &r = 0.017569 \text{ dyn sec/cm}^3 , \end{aligned} \quad \text{(C11)}$$

from the assumed impedance parameters

$$\begin{aligned} &K(x) = 10^9 e^{-2ax} \text{ dyn/cm}^2 , \\ &R(x) = 300\, e^{-ax} \text{ dyn sec/cm}^2 , \\ &a = 1.7 , \\ &M = 0.05 \text{ gm/cm} , \\ &L = 3.5 \text{ cm} , \\ &H = 0.1 \text{ cm.} \end{aligned} \quad \text{(C12)}$$

It is interesting to observe what might happen if one could drain all chambers of the cochlea without causing any damage. If this were possible, the eigenfrequencies of the BM would be given by those frequencies where Z is zero. The resonant frequency f, bandwidth BW, and the quality factor Q may then be found using the results of (C12)

$$f_0 = 1/2\pi[K(x)/M - (R(x)/2M)^2]^{1/2} \text{ Hz} ,$$
$$\text{BW} = R(x)/M \text{ Hz} , \quad \text{(C13)}$$
$$Q = f_0/\text{BW} \simeq M/2\pi R(x)[K(x)/M]^{1/2} .$$

This calculation gives values for the Q of about 3.75. This value of the Q seems intuitively reasonable given the transverse fiber material discussed by Iurato (1967). A direct measurement of the unloaded Q of the basilar membrane would obviously be very useful in increasing our understanding of possible internal loss mechanisms. A measurement of this kind might also give an increased insight into nonlinear effects if the nonlinearity is in the loss term, and if the loss is due to internal friction.

APPENDIX D: DERIVATION OF THE INTEGRAL EQUATION

We may transform the differential equation to an equivalent integral-equation formulation by the following procedure (Green's-function method).

Define $G(X|X')$ by the differential equation

$$\nabla^2 G(X|X') = -\delta(X - X') . \quad \text{(D1)}$$

Upon integrating the combination

$$\phi\nabla^2 G - G\nabla^2\phi \quad \text{(D2)}$$

by parts, one may show that

$$\phi(X) = \int_{S'} G(X|X')\frac{\partial\phi}{\partial n'}dS' - \int_{S'}\phi(X')\frac{\partial G}{\partial n'}dS' , \quad \text{(D3)}$$

where $\phi(X)$ is the potential and

$$-\partial\phi/\partial n \quad \text{(D4)}$$

is the normal velocity of the fluid out of the surface. S' is the surface of the container.

Finally, by assuming the boundary conditions of $G(X|X')$ to be

$$\partial G/\partial n'|_{X' \text{ on } S'} = 0 , \quad \text{(D5)}$$

we may reduce (D3) to the simpler form

$$\phi(X) = -\int_{S'} G(X|X')V_n(X')dS' , \quad \text{(D6)}$$

where we have defined the normal velocity $V_n(X)$ to be out of the box.

All normal velocities are zero except on $x = 0$, $x = 2L$, and on the BM. Since $V_n = -1$ on the end $x = 0$ and 1 at $x = 2L$, we may find an expression for the potential on the surface of the basilar membrane $y = 0$:

$$\phi(x) = \int_{x'=0}^{2L} G(x, 0|x', 0)V_y(x', 0)dx' - \int_{y'=0}^{H}[G(x, 0|2L_x, y') - G(x, 0|0, y')]dy' , \quad \text{(D7)}$$

where $V_y(x)$ is the velocity of the BM at x, $y = 0$. The dependence on z has been suppressed in this derivation since we assume an infinite extent in this direction (two-dimensional model).

TABLE E-I. Data for Appendix E.

x	ϕ_r	ϕ_i	V_r	V_i
0.00	−0.6515	0.7440	−0.2572E−01	0.2948E−01
0.18	−0.4733	0.7412	−0.3397E−01	0.5349E−01
0.35	−0.2846	0.7217	−0.3707E−01	0.9497E−01
0.53	−0.8355E−01	0.6718	−0.1932E−01	0.1615
0.70	0.1244	0.5702	0.5650E−01	0.2512
0.88	0.3155	0.3885	0.2605	0.3151
1.06	0.4252	0.1057	0.6555	0.1544
1.23	0.3257	−0.2295	0.9593	−0.7014
1.41	−0.8795E−01	−0.3363	−0.5991	−2.062
1.58	−0.2299	0.2383	−3.275	3.743
1.76	−0.1990	−0.2623E−02	−13.78	2.167
1.93	0.8599E−04	−0.5591E−04	−0.6188E−02	0.3039E−02
2.11	0.1642E−04	−0.7212E−05	−0.5453E−03	0.2120E−03
2.29	−0.4139E−05	−0.6315E−05	0.1011E−03	0.1630E−03
2.46	−0.1516E−04	0.1191E−04	0.3477E−03	−0.2640E−03
2.64	−0.9431E−05	0.7807E−05	0.2035E−03	−0.1645E−03
2.81	−0.4497E−05	0.1577E−04	0.9595E−04	−0.3262E−03
2.99	−0.6338E−05	0.1651E−04	0.1313E−03	−0.3360E−03
3.17	0.2045E−04	−0.6115E−05	−0.4140E−03	0.1218E−03
3.34	0.5713E−05	−0.9545E−05	−0.1156E−03	0.1917E−03
3.50	0.0000	0.0000	0.0000	0.0000

Finally to simplify the notation, we define

$$G_s(x|y') = G(x, 0|0, y') , \quad \text{(D8)}$$
$$G_{BM}(x|x') = G(x, 0|x', 0) , \quad \text{(D9)}$$

and

$$V_{BM}(x) = V_y(x, 0) . \quad \text{(D10)}$$

Thus (D7) may be written as

$$\phi(x) = +2\int_{y'=0}^{H} G_s(x|y')dy' + 2\int_{x'=0}^{L} G_{BM}(x|x')V_{BM}(x')dx' , \quad \text{(D11)}$$

where we have used the symmetry of G_{BM} and V_{BM} to reduce the integration limits of both integrals.

APPENDIX E

In Table E-I we present a few values of the potential $\phi(x)$ and the velocity $V_{BM}(x)$ for the case of $f = 1000$ Hz. Conditions were as described in the text by Eq. (C12). The length of the cochlea L was assumed to be 3.5 cm and the height H was 0.1. Of the 200 points used, we list only one out of every ten, starting with the first at $x = 0$. ρ is 1.

APPENDIX F: SUMMARY OF FINAL EQUATIONS

A. Basic equation

$$\phi(x) + 2i\omega\rho\int_{x'=0}^{L} G_{BM}(x|x')\frac{\phi(x')}{Z(x', \omega)}dx' = L - x . \quad \text{(13)}$$

B. Green's function

$$G_{BM}(x|x') = \frac{-1}{\pi}\sum_{n=-\infty}^{\infty}\sum_{m=-\infty}^{\infty}(-1)^n \ln(r_{nm}^{+}r_{nm}^{-}) \quad \text{(B4)}$$

$$r_{nm}^{\pm} = [(x \pm x' + 2nL)^2 + (2mH)^2]^{1/2} . \quad \text{(B5)}$$

C. Impedance

$$Z(x, \omega) = K(x)/i\omega + i\omega M + R(x) . \quad \text{(C10)}$$

D. Velocity, pressure

$$V_{BM}(x,\omega) = -i\omega\rho\phi(x,\omega)/Z(x,\omega)\,,$$
$$p(x,\omega) = i\omega\rho\phi(x,\omega)\quad . \tag{3}$$

[1]The characteristic place is defined as the point of maximal displacement for a single-frequency input.
[2]The following method of solution may be generalized to include the effects of fluid compressibility, but the generalization appears to be unnecessary.
[3]It is easy to check that if ϕ is zero on the plane $x = L$ then V_y is zero on that surface as required by the antisymmetric condition.
[4]The velocity potential is proportional to the pressure as shown by Eq. (3).

Physical measurements

Iurato, S. (1967). *Submicroscopic Structure of the Inner Ear*, edited by S. Iurato (Pergamon, New York).
Johnstone, B. M., and Boyle, A. J. F. (1967), "Basilar Membrane Vibrations Examined with the Mössbauer Technique," Science 158, 389–390.
Rhode, W. S. (1971). "Observations of the Vibration of the Basilar Membrane in Squirrel Monkeys using the Mössbauer Technique," J. Acoust. Soc. Am. 49, 1218–1231.
Rhode, W. S., and Robles, L. (1974). "Evidence from Mössbauer experiments for nonlinear vibration in the cochlea," J. Acoust. Soc. Am. 55, 588–596.
von Békésy, Georg (1960). *Experiments in Hearing* (McGraw–Hill, New York).
Wilson, J. P., and Johnstone, J. R. (1972). "Capacitive Probe Measurements of Basilar Membrane Vibration," Symposium on Hearing Theory, 172–181. IPO. Eindhoven, Holland.

One-Dimensional Models

Peterson, L. C., and Bogert, B. P. (1950). "A Dynamical Theory of the Cochlea," J. Acoust. Soc. Am. 22, 369–381.
Schroeder, M. R., (1973). "An Integrable Model for the Basilar Membrane," J. Acoust. Soc. Am. 53, 429–434.
Zweig, G., Lipes, R., and Pierce, J. R. (1976). "The Cochlear Compromise," J. Acoust. Soc. Am. 59, 975–982.
Zwislocki, J. J. (1965). "Analysis of some auditory characteristics," *Handbook of Mathematical Psychology*, edited by R. D. Luce, R. R. Bush, and E. Galanter (Wiley, New York),pp. 1–98.

Multidimensional models

Lien, M. D., and Cox, J. R. (1973). "A Mathematical Model of the Mechanics of the Cochlea," PhD dissertation (Sever Institute of Washington University, St. Louis, MO) (unpublished).
Lesser, M. B., and Berkley, D. A. (1972). "Fluid Mechanics of the Cochlea. Part 1," J. Fluid Mech. 51, part 3, 497–512.
Ranke, O. F. (1950). "Theory of operation of the Cochlea: a contribution to the hydrodynamics of the cochlea," J. Acoust. Soc. Am. 22, 772–777 (1950).
Siebert, W. M. (1974). "Ranke Revisited—A Simple Short-wave Cochlea Model," J. Acoust. Soc. Am. 56, 594–600.
Steele, C. R., (1974). "Behavior of the Basilar Membrane with Pure tone Excitation," J. Acoust. Soc. Am. 148–162.

Basilar-Membrane models

Allarie, P., Raynor, S., and Billone, M., (1974). "Cochlea Partition Stiffness—a Composite Beam Model," J. Acoust. Soc. Am. 55, 1252–1258.
Novoselova, S. M. (1975). "The Basilar Membrane as an Elastic Plate," Sov. Phys. Acoust. 21, 56–60.

Nonlinear models

Hall, J. L. (1974). "Two-tone distortion products in a nonlinear model of the basilar membrane," J. Acoust. Soc. Am. 1818–1828.
Hubbard, A. E., and Geisler, C. D. (1972). "A hybrid-computer model for the cochlear partition," J. Acoust. Soc. Am. 51, 1895–1903.
Kim, D. O., Molnar, C. E., and Pfeiffer, R. R. (1973). "A System of Nonlinear Differential Equations Modeling Basilar-Membrane Motion," J. Acoust. Soc. Am. 54, 1517–1529.

General

Morse, P. M., and Feshbach, H. (1953). *Methods of Theoretical Physics* (McGraw–Hill, New York) Part I, p. 814.
Schroeder, M. R. (1975). "Models of Hearing," Proc. IEEE 63, 1332–1350.
Timoshenko, S., and Woinowsky–Krieger, S. (1959). *Theory of Plates and Shells* (McGraw–Hill, New York).

Two-dimensional cochlear fluid model: New results

J. B. Allen

Citation: The Journal of the Acoustical Society of America **61**, 110 (1977); doi: 10.1121/1.381272
View online: https://doi.org/10.1121/1.381272
View Table of Contents: https://asa.scitation.org/toc/jas/61/1
Published by the Acoustical Society of America